Accelerated tumor progression in mice lacking the ATP receptor P2X7

Elena Adinolfi[1*], Marina Capece[1*], Alessia Franceschini[1], Simonetta Falzoni[1], Anna Lisa Giuliani[1], Alessandra Rotondo[1], Alba Clara Sarti[1], Massimo Bonora[1], Susanne Syberg[2], Domenica Corigliano[3], Paolo Pinton[1], Niklas R Jorgensen[2], Luigi Abelli[4], Laura Emionite[5], Lizzia Raffaghello[6], Vito Pistoia[6], and Francesco Di Virgilio[1]

[1]Department of Morphology, Surgery and Experimental Medicine, Section of Pathology, Oncology and Experimental Biology, University of Ferrara, Italy.

[2]Research Center for Ageing and Osteoporosis, Departments of Diagnostics and Medicine, Glostrup Hospital, University of Copenhagen, 2600 Glostrup, Denmark.

[3]Department of Health Sciences, Università della Magna Grecia, Catanzaro, Italy.

[4]Department of Life Sciences and Biotechnology, Section of Biology and Evolution, University of Ferrara, Italy.

[5]Animal Facility, S. Martino Hospital, Genova, Italy

[6]Laboratory of Oncology, Gaslini Hospital, Genova, Italy.

*Elena Adinolfi and Marina Capece equally contributed to this paper.

Running Title: P2X7 and cancer.

Keywords: P2X7; extracellular ATP; purinergic signalling; inflammation.

Grant Support: FDV is supported by grants from the AIRC (n. IG 5354), Telethon (n. GGP06070), ERA-NET Neuron "Nanostroke", the Ministry of Health of Italy (n. RF-2011-02348435), the Italian Ministry of Education, University and Research (n. RBAP11FXBC_001) and

funds from the University of Ferrara. FDV and NRJ were also supported by the 7th Framework Program HEALTH-F2-2007-202231 "ATPBone". PP is supported by grants from AIRC (IG 14442), and the Italian Ministry of Education, University and Research (COFIN n. 20129JLHSY_002, FIRB n. RBAP11FXBC_002, and Futuro in Ricerca n. RBFR10EGVP_001). EA is a recipient of a My First AIRC Grant (MFAG, n. 11630) and a Young Investigator Grant "Alessandro Liberati" from Regione Emilia-Romagna.

Corresponding author: Dr Francesco Di Virgilio, e-mail: fdv@unife.it; phone +39 0532 455353

Conflict of interest: The Authors declare no potential conflict of interest.

Word count: 5490

Total number of Figures: 7

Supplementary material: 3 Figures plus 2 movies.

Abstract

The ATP receptor P2X7 (P2X7R or P2RX7) has a key role in inflammation and immunity, but its possible roles in cancer are not firmly established. In the present study we investigated the effect of host genetic deletion of P2X7R in the mouse on the growth of B16 melanoma or CT26 colon carcinoma cells. Tumor size and metastatic dissemination were assessed by *in vivo* calliper and luciferase luminescence emission measurements along with *post-mortem* examination. In P2X7R-deficient mice, tumor growth and metastatic spreading were accelerated strongly compared to wild-type (wt) mice. Intratumoral IL-1β and VEGF release were drastically reduced and inflammatory cell infiltration was abrogated nearly completely. Similarly, tumor growth was also greatly accelerated in wt chimeric mice implanted with P2X7R-deficient bone-marrow cells, defining hematopoietic cells as a sufficient site of P2X7R action. Finally, dendritic cells (DCs) from P2X7R-deficient mice were unresponsive to stimulation with tumor cells, and chemotaxis of P2X7R-less cells was impaired. Overall, our results showed that host P2X7R expression was critical to support an anti-tumor immune response, and to restrict tumor growth and metastatic diffusion.

Introduction

Receptors for extracellular nucleotides are named P2 receptors (P2Rs) (1). P2Rs are further subdivided into P2YRs and P2XRs. The P2X7 receptor (P2X7R), a member of the P2XRs subfamily, can function as a cation-selective ion channel or as non-selective plasma membrane pore, and is heavily implicated in inflammation and immune-modulation (2) (3). Opening of the non-selective P2X7R pore is most often associated to cytotoxicity. However, P2X7R expression also supports tumor growth, both in allogeneic (*nude/nude* host) and syngeneic models, while P2X7R blockade inhibits tumor growth (4), (5). These experiments suggested that P2X7R antagonists might be novel potential anticancer drugs. However, accumulating evidence shows that P2X7R is needed to support Ag presentation to $CD4^+$ lymphocytes by tumor-associated dendritic cells (DCs) (6), (7), thus the question arises as to what extent host P2X7R is needed to control tumor growth, and if P2X7R blockade might impair the anti-tumor immune response. Previous studies show that genetic deletion of P2X7R prevents graft-versus-host-disease (GVHD) (8), and that P2X7R blockade prevents rejection of allogeneic transplants (9), (10).

To clarify the role of the P2X7R in host-tumor interaction, we investigated tumor growth and metastatic spreading in syngeneic wt and *p2x7R*$^{-/-}$ hosts. As tumor models, we used B16 melanoma and CT26 colon carcinoma cells inoculated into C57Bl/6 or BALB/cJ mice, respectively. In the light of previous data showing that tumors expressing the P2X7R have a much faster growth kinetic *in vivo* (5), we also explored whether silencing tumor P2X7R affected tumor growth in the *p2x7R*$^{-/-}$ host. Our data show that expression of host P2X7R was a crucial factor in anti-tumor response as in its absence tumor growth and metastatic spreading were dramatically accelerated. Tumors growing in the *p2x7R*$^{-/-}$ host showed virtually no inflammatory infiltrate and modest IL-1β and VEGF release. Lack of inflammatory infiltrate was likely due to inability of immune cells from the P2X7R-deleted host to respond to tumor cells. This conclusion is also supported by bone-marrow transfer (BMT) experiments showing that in P2X7R-wt chimeric mice reconstituted with

P2X7R-KO bone-marrow tumor growth kinetic is very similar to that observed in P2X7R-KO mice.

Altogether these data unveil a novel function of P2X7R in the control of tumor growth.

Materials and Methods

Reagents and antibodies

Tris base, sodium chloride, Triton X-100, RPMI, non essential aminoacidics, hygromycin, haematoxylin, eosin, ethanol, Bouin fixative solution, rabbit polyclonal anti-P2X7 antibody (P8232) were from Sigma-Aldrich (Milan, Italy). FBS, penicillin and streptommycin solution were from Euroclone (Milan, Italy). H_2O_2 and xylene were from Carlo Erba (Rodano, Italy). 3,3'-diaminobenzidine (DAB) chromogen solution, Target Retrieval solution, horse radish peroxidase (HRP)- conjugated goat anti-rabbit were from Dako (Dako Italia, Milano, Italy). Anti-F4/80 (CI:A3-1) and sheep anti-rat HRP-conjugated IgG, were from Tema Ricerca (Bologna, Italy). Rabbit polyclonal anti-CD3 (ab5690), rat monoclonal (ab22378) anti-CD8, and anti-VEGF (ab46154) Abs were from Abcam (Cambridge, UK). Mouse VEGF and mouse IL1β/IL-1F2 Quantikine ELISA kits were from R&D systems (Minneapolis, MN, USA). AZ10606120 dihydrochloride and A74003 were from Tocris Bioscience (Bristol, UK). Red blood cell lysis buffer was from Sigma-Aldrich, while Recombinant Murine (rm) GM-CSF was from PeproTech (London, UK).

Cell cultures

B16 melanoma and CT26 colon carcinoma cells were a kind gift of Drs M.P. Colombo (Istituto Nazionale Tumori, Milano) and Guido Kroemer (INSERM, Paris), respectively, and extensively tested in the Authors laboratories (11) (12). The N13 microglial cell was a kind gift of Dr Paola Ricciardi-Castagnoli (Singapore Immunology Network, Singapore), and extensively tested in the Authors laboratory for cytokine and surface marker expression (13). The luc2 luciferase expression vector (pGL4.50/hygro) was from Promega (Madison, WI, USA). The P2X7shRNA in pSuper.neo.GFP vector was a gift of Dr. Miguel Diaz-Hernandez, Universidad Complutense,

Madrid, Spain (14). Stably transfected cell lines were obtained by selection with either hygromicyn (0,1-0,2 mg/ml) or G418 sulfate (0.2-0.8 mg/ml) (Calbiochem, La Jolla, CA, USA).

Mice strains, tumor generation, *in vivo* imaging and drug administration

In vivo experiments were performed with two different *p2x7*$^{-/-}$ mouse strains and corresponding wt controls: C57Bl/6, a gift from GlaxoSmithKline (Stevenage, UK), and BALB/cJ (15). Five x 10^5 B16, or 2.5 x 10^5 CT26 cells were subcutaneously (s.c.) inoculated into C57Bl/6 or BALB/cJ mice, respectively. Tumor size was measured with a calliper, and volume calculated according to the following equation: volume = $\pi/6$ [w1 x $(w2)^2$], were w1= major diameter and w2= minor diameter. Blood samples were obtained by *post mortem* beheading. Luciferase luminescence was followed with a total body luminometer (IVIS Lumina, Caliper-Perkin Elmer, Hopkinton, MA, USA). Mice were anesthetized with 2.5% isofluorane, i.p. injected with 150 mg/kg D-luciferin (Perkin Elmer), and luminescence quantified after 15 min using the Living Image® software (Caliper). Lung metastases were obtained by intravenous (i.v.) injection of B16 cells. P2X7R antagonists or vehicle (sterile PBS containing 0.005% DMSO) were i.p. injected (100 μl) every two days after first tumor mass detection. Animal procedures were approved by the University of Ferrara ethic committee and the Italian Ministry of Health in compliance with international laws and policies (European Economic Community Council Directive 86/109, OJL 358, Dec. 1, 1987, and NIH Guide for the Care and Use of Laboratory Animals).

Bone-marrow transplantation and tumor growth in P2X7R-wt and P2X7R-KO mice

P2X7R-wt and P2X7-KO$^-$ mice on a BALB/cJ background were treated with Treosulfan (Medec Gmbrl, Hamburg, Germany) (1.5 g/kg/day) for 3 consecutive days. Treosulfan was used as a single agent for conditioning prior to BMT to achieve myeloablation as described (16). Recipient mice were injected i.v. with 1×10^7-nucleated cells obtained from P2X7R-wt or P2X7-KO donors.

Bone-marrow cells were obtained by flushing the cavity of freshly dissected femurs with sterile 0.9% NaCl saline solution. Cells were dispersed by pipetting, washed, counted, resuspended in saline and i.v. injected, as described by Sangaletti et al. (17). To verify engraftment, peripherally blood mononuclear cells withdrawn from the retro-orbital sinus six weeks after BMT were resuspended in TRIzol® LS Reagent (Ambion®, LifeTechnology, Monza, Italy) for RNA isolation and evaluated for P2X7 expression by qRT-PCR. Eight weeks after BMT, mice were s.c. inoculated in the right hip with CT26 murine colon carcinoma cells (250.000 cells/mouse).

IL-1β assay

Mouse plasma was collected after blood centrifugation (1000 x *g*, 10 min at 4° C). Tumor specimens were homogenated in lysis buffer (300 mM sucrose, 1 mM K_2HPO_4, 5.5 mM D-glucose, 20 mM Hepes, 1 mM phenylmethylsulfonyl fluoride, 1 mM benzamidine, 0.5% IGEPAL) with a Potter pestle. Two x 10^5 B16 or B16shRNA cells, were seeded into 24 well culture dishes in complete RPMI, incubated for 24 hours in the same medium, and supernatants assayed for IL1β content.

Isolation of bone marrow-derived DCs and peritoneal macrophages from wt and P2X7R-KO mice

Bone marrow cells were obtained as previously described (18) (19). Tibiae and femurs from 6 week old mice were removed, cut and the marrow flushed with RPMI. The cell suspension was collected and washed with RPMI by 10 min centrifugation at 1100 rpm. Cells were incubated for 5 min at room temperature in red blood cell lysis buffer (Sigma-Aldrich). Reaction was stopped by adding RPMI, cells were centrifuged, resuspended in rm-GM-CSF-supplemented (20 ng/ml) RPMI, and seeded in Petri dishes at a concentration of $2.5x10^5$ cells/ml. At day 10 DCs were collected, and seeded at a concentration of $1x10^5$ cells/ml in the presence or absence of $1x10^5$ B16-wt cells/ml. Supernatants were collected and assayed for IL-1β content. Peritoneal macrophages were isolated

as described (20). Mice were killed by excess anesthesia, and 4.5 ml sterile PBS was injected into the peritoneal cavity. The peritoneum was gently massaged, and fluid recovered. Peritoneal macrophages were collected by centrifugation at 200 × *g* for 5 min at 4°C.

Histology and immunohistochemistry

Tumors were fixed in Bouin's fixative for 7 hours at 4 °C, dehydrated in cold-graded ethanol series, cleared in xylene and embedded in paraffin. Serial 7 µm-thick sections were stained with haematoxylin/eosin (H/E). For immunohistochemistry of CD3, F4/80 and VEGF, sections were rehydrated, washed in Tris-buffered saline (TBS, 150 mM NaCl supplemented with 50 mM Tris, pH 7.6), blocked for 1 hour in TBS containing 10% FCS and 1% BSA, incubated for 16 hours at 4 °C with TBS containing 1% BSA and the diluted primary antibodies (anti-CD3 or anti-VEGF rabbit polyclonal antisera, both at 1:100, anti-F4/80 rat mAb, 1:80, CD8, 1:50). For immunohistochemical detection of CD8, heat-induced epitope retrieval was performed using Dako Target Retrieval solution. Slides were then washed twice in TBS containing 0.025% Triton X-100, and endogenous peroxidase activity was blocked by a 20 min incubation at room temperature in 0.3% H_2O_2-containing TBS. Sections were then incubated for 1 hour at room temperature with 1% BSA-containing TBS, and the diluted secondary antibodies (HRP-conjugated goat anti-rabbit IgG, 1:200, or sheep anti-rat IgG, 1:1000). Tissue sections were washed twice in TBS, and peroxidase activity detected with Liquid DAB Substrate Chromogen System (Dako). Nuclear counterstaining was performed with Mayer's hematoxylin. Sections were dehydrated, mounted with EUKITT (Kindler GmbH, Freiburg, Germany), and images acquired and analysed with a Nikon eclipse 90i digital microscope equipped with a NIS-elements software (Nikon Instruments Europe, Anstelveen, The Netherlands).

Wound-healing assay

Cell migration was investigated by wound-healing assay. Cells were seeded in Petri dishes at a concentration of 2.5 x 10^5/ml, grown to confluence and scratched with a sterile pipette tip to generate wounding across the cell monolayer. Cell migration was observed in a sealed and thermostatted (37°C) chamber, at controlled CO_2 concentration (5%), across a wound spanning 100 μm. Images were acquired for 16 h using a Nikon Swept Field Confocal system, at 20x magnification under transmitted light. Images were then analyzed using open source ImageJ Fiji software.

Statistics

Unless otherwise stated, data are shown as mean ± SE of the mean, and test of significance was performed with Student's t test using Graphpad InStat (GraphPad Software Inc, San Diego, CA, USA).

Results

Lack of the P2X7R prevents GVHD (8) and P2X7R targeting increases long-term survival of heart and pancreatic islets transplants (9), (10). Thus, we hypothesized that host P2X7R deletion might facilitate tumor progression. To investigate host-tumor interaction in the P2X7R-deleted host, we used B16 mouse melanoma and CT26 mouse colon carcinoma cells. B16 cells were also stably transfected with a cytosolic luciferase construct to allow *in vivo* tumor progression. Lack of P2X7R did not affect B16 or CT26 engrafting. Tumor growth, assessed by calliper, was barely measurable up to post-injection (p.i.) day 6 in both wt and P2X7R-KO mice. After p.i. day 9, growth kinetic was much faster in the P2X7R-deleted than in the wt host, as tumors were three fold larger in the KO than in the wt host (Fig. 1A). Larger size of tumors from P2X7R-deleted host was confirmed at *post-mortem* analysis (Fig. 1B, upper panel). Expression of P2X7R by transplanted tumors has a pronounced growth-promoting effect (5). To test whether P2X7R expression by the tumor cells might affect tumor growth in the P2X7R-deleted host we generated stable P2X7R-silenced (P2X7R shRNA) B16 cell clones. Characteristics of P2X7R-silenced B16 cells are reported in Supplementary Fig. S1. As shown in Fig. 1A, silencing tumor P2X7R caused a profound inhibition of tumor growth, slightly stronger in P2X7R-wt than in P2X7R-KO mice. At p.i. day 14, tumors masses generated by P2X7R-silenced B16 cells were several fold smaller than tumors generated by B16 wt cells. Size of tumors generated by silenced B16 cells in wt and P2X7R-KO mice is shown in Fig. 1B, lower panel.

Bioluminescence analysis allowed tumor detection in both mouse strains at least four days earlier than calliper measurement, i.e. at p.i. day 5, vs p.i. day 9 (Fig. 1C and D). Regrettably, bioluminescence measurements were reliable for only about 10-12 days, and up to a tumor size of about 1000 mm^3. At later time points, photon emission declined and luminescence intensity did not correlate with the effective tumor size measured by calliper (Fig. 1D). Apparent decrease in size of tumors growing in the P2X7R-KO host was due to massive intra-mass hemorrhagic necrosis that

drastically reduced tumor cell number, thus decreasing luminescence emission (Supplementary Fig. S2).

To explore the effect of P2X7R deletion in a mouse strain of a different genetic background and in a different tumor, BALB/cJ mice were inoculated with the syngeneic CT26 colon carcinoma. Also in the BALB/cJ model P2X7R deletion caused an acceleration of tumor growth (Fig. 1E). *Ex-vivo* measurement of excised masses confirmed the *in vivo* measurements (Fig. 1F and G). Effect of P2X7R deletion on tumor growth was stronger in the BALB/cJ than in the C57Bl/6 mice. Up to p.i. day 13, the CT26 tumor (BALB/cJ host) was almost 5-6 fold larger in the P2X7R-KO than in the wt mice, while over the same time span the B16 tumor (C57Bl/6 host) was only 2-3 fold larger in the P2X7R-KO than in the wt. This might also depend on the different *p2x7R* genetic variant expressed in the two mouse strains. In fact, C57Bl/6 mice are homozygous for an allelic loss-of-function mutation (P451L) that decreases P2X7R activity, while BALB/cJ mice carry the fully functional wt *p2x7R* alleles (P451) (21). Thus, P2X7R-dependent responses in C57Bl/6-wt are about 50% weaker than those of BALB/cJ-wt, i.e. closer to the KO phenotype of both strains.

We then set to investigate whether lack of host P2X7R might affect metastatic efficiency. Fig. 2A and B show *in vivo* bioluminescence emission from mice i.v. injected with B16 cells. In 3 out of 6 P2X7-KO, but in none of the wt mice, luminescence emission from the thoracic cage was detectable at p.i. day 18. Fig. 2C, reports a time course of luminescence emission from mice # 11 (wt) and # 4 (KO) showing that lung metastases were clearly detectable in the KO animal as early as p.i. day 15, but only at p.i. day 21 in the wt. By this time, luminescence in the KO mouse had spread all over the thoracic cage. At p.i. day 21, mice were sacrificed and lungs examined for metastases. Fig. 2D shows that number of metastatic foci in the lungs from the KO mouse was much higher than in the wt. Average lung metastases number from the two strains is shown in Fig. 2E. In mice inoculated with P2X7R-silenced tumors only 1-2 metastases per lung, irrespectively of the genetic background, were found (not shown).

Infiltration by inflammatory cells is a constant feature of malignant tumors. To our surprise, histology of B16 tumors from P2X7-KO mice showed very little if any inflammatory infiltrate, whether at the tumor/connective tissue interface or within the tumor mass (Fig. 3A-C). On the contrary, tumors growing in wt mice showed, as expected, a massive inflammatory infiltrate in the peritumoral connective tissue (Fig. 3D), at the tumor/connective tissue interface (Fig. 3E) and within the tumor itself (Fig. 3F). Tumors were also stained with anti-CD3 and anti-F4/80 Abs to highlight the presence of T lymphocytes and macrophages/DCs. As shown in Fig. 4A and C, few if any T lymphocytes or mononuclear phagocytes were identified in specimens from the KO mice. See for comparison specimens from wt mice (Fig. 4B and D). The tumor-infiltrating T lymphocyte population in the P2X7R-wt host was largely made by $CD8^+$ cells, as shown by specific staining in Fig. 4E and F. No $CD8^+$ positive cells were detected in tumor specimens from P2X7R-KO mice (not shown).

Lungs from the KO animal showed virtually no inflammatory infiltrate, whether at site of metastases or in the distal lung tissue (Fig. 5A and B). Other signs of inflammation, i.e. thickening of alveolar septa or increased number of alveolar macrophages, were also missing. On the contrary, lungs from wt mice showed diffuse signs of inflammation (Fig. 5D and E). CD3 immunostaining showed T lymphocyte infiltration in the metastases from the wt (Fig. 5F) but not from the KO mouse (Fig. 5C).

Absence of inflammatory infiltrate suggested that accelerated tumor growth in the P2X7R-KO host might be due to inefficient immune response. Thus, we investigated the effect of selective P2X7R deletion on hematopoietic cells by generating BALB/cJ P2X7R chimeric mice. Chimeras were obtained by inoculating P2X7R-KO bone-marrow into P2X7R-wt recipient mice (P2X7R-KO>P2X7R-wt chimeras), or on the contrary P2X7R-wt bone-marrow into P2X7R-KO mice (P2X7R-wt>P2X7R-KO chimeras). We also reconstituted P2X7R-KO recipients with P2X7R-KO bone marrow (P2X7R-KO>P2X7R-KO mice) and P2X7R-wt recipients with P2X7R-wt bone marrow recipients (P2X7R-wt>P2X7R-wt) as a control. As shown in Fig. 6A, tumor proliferated to

a higher rate in P2X7R-KO>P2X7R-wt than in P2X7R-wt>P2X7R-wt or P2X7R-wt>P2X7R-KO chimeras, indicating that lack of P2X7R expression on immune cells was a main cause for the accelerated growth observed in the P2X7R-deleted host.

A main P2X7R-dependent response is IL-1β release, a cytokine crucial in host-tumor interactions. An increase in IL-1β plasma levels is considered a poor prognostic factor in melanoma (22), (23). Fig. 6B, shows that blood IL-1β levels in tumor-bearing wt mice were about twice as high as in P2X7R-KO mice. A low in IL-1β serum level in the P2X7R-KO mice was anticipated, as this receptor is a near absolute requirement for IL-1β release evoked by many different stimuli (24), (25), (26), (27). Since melanomas are a source of IL-1β (23), P2X7R deletion did not entirely suppress serum levels of this cytokine. Next, we analyzed IL-1β content of excised tumor masses. As shown in Fig. 6C, tumors from KO mice contained IL-1β to an at least four-fold lower amount compared to tumors from wt animals. Interleukin-1β content of tumors generated by P2X7R-silenced B16 cells was reduced in the wt and nearly abolished in the KO host (Fig. 6C). Reduced intra-mass IL-1β content suggested that lack of P2X7R impaired tumor interaction with host immune cells. To test this hypothesis, DCs were isolated from mouse bone-marrow and challenged with B16 cells. As shown in Fig. 6D, challenge of DCs from wt mice triggered a large IL-1β release, that was reduced to about one third in DCs from P2X7R-KO mice.

We recently showed that secretion of VEGF is critically dependent on P2X7R (5). As shown in Supplementary Fig. S3, B16 cells *in vitro* released VEGF in a P2X7R-dependent fashion. Tumors from P2X7R-KO animals had 50% lower VEGF compared to wt mice. P2X7R-silencing further reduced VEGF content in both mice strains. Lower VEGF content in tumors from P2X7R-KO mice was confirmed by immunohistochemistry (Supplementary Fig. S3). Pharmacological P2X7R blockade or silencing have a strong anti-tumor effect (5). In these original experiments P2X7R blockers were administered directly into the tumor mass, thus maximizing blockade of tumor rather than host P2X7R (5). This administration route might mask possible untoward effects

due to host P2X7R blockade, and possibly be unpractical for anti-cancer therapy. To tackle this objection, two selective P2X7R blockers were intra-peritoneally (i.p.) administered to P2X7R-wt tumor bearing mice. As shown in Fig. 6E-G, both blockers had a strong inhibitory effect on tumor growth compared to vehicle, thus showing that P2X7R blockers have a strong anti-cancer activity even when systemically administered. As expected, administration of P2X7R blockers had no effect on the growth of tumors lacking P2X7R (not shown).

Lower intra-tumor IL-1β levels might explain a reduced inflammatory infiltrate, however lack of inflammation found in the P2X7R-KO mice was so striking that we hypothesized that P2X7R deletion might cause a more profound defect in immune cell migration. Thus, we performed an *in vitro* wound healing experiment with peritoneal macrophages from wt and KO mice as well as the N13 mouse microglial cells. N13 cells have been widely used to study P2X7R responses, and from this cell line we selected several clones lacking P2X7R (13). One of such clones, N13R, was used in the experiments shown in Fig. 7A-F. N13-wt and N13R cells were layered in a culture dish and, after reaching confluence, the monolayer was wounded with a pipette tip. N13-wt microglia cells migrated from both sides of the wound and within 12 h re-established continuity of the monolayer. On the contrary, N13R cells were unable to repopulate the wound. As shown in the Supplementary movies (Supplementary Movies S4 and S5), N13R cells were motile, but incapable of directional migration. Peritoneal macrophages yielded similar results but speed of repopulation of the scratch was slower compared with microglia. In agreement with the N13R data, macrophages from P2X7R-KO mice were unable to migrate into the scratch (not shown). These experiments suggested that lack of P2X7R hinders the ability of inflammatory cells to chemotact, and thus infiltrate the tumor.

Discussion

The tumor microenvironment, a key factor in anti-cancer host immune response, is rich in inflammatory cells, pro-inflammatory, immunosuppressive and angiogenic factors, among which extracellular ATP (28) (29), (12). Under physiological conditions, and in healthy tissues, the extracellular ATP concentration is in the nanomolar range (30), to increase to the hundred micromolar level at inflammatory or tumor sites, where it drives migration of inflammatory cells, release of cytokines, stimulation of tumor cell proliferation, and generation of adenosine. (29), (12), (31).

Expression by host and tumor cells of different purinergic receptor subtypes with widely different affinity confers to purinergic signalling an astonishing plasticity. However, most subtypes have high affinity for extracellular nucleotides, suggesting that within tumors they must be desensitized. This is not the case for the P2X7R, thanks to its low affinity for ATP (EC50 in the 100-300 μM range) and its non-desensitizing behaviour (32), (33). P2X7R triggers IL-1β secretion, ROS generation, metalloprotease release and intracellular pathogen killing (7), (34), (35). In addition, P2X7R overactivation causes cell death (36), (37). On the other hand, tonic stimulation of P2X7R by endogenously-released ATP, i.e. in the absence of pharmacological ATP doses, supports growth (38), (39), (40), (5). Thus, it is anticipated that P2X7R should be active on both the tumor and the host cells, with a final outcome difficult to anticipate.

Most tumors express P2X7R to high level, and are dependent on its function for growth and metastatization (4), (41). In tumor cells, P2X7R is constantly and tonically active, thus causing: a) moderate increase in the endoplasmic reticulum and mitochondrial Ca^{2+} concentration, b) enhanced efficiency of oxidative phosphorylation; c) increase in intracellular ATP stores, d) activation of the transcription factor NFATc1, e) stimulation of aerobic glycolysis, and f) stimulation of proliferation (5), (38), (40), (42), (43).

Here we investigated the role of host P2X7R in anti-tumor response. By using two different P2X7R-KO mouse strains, we show that expression of host P2X7R is an absolute requirement for

anti-tumor response. B16 melanoma cells proliferated to a rate two-fold faster in the *p2x7R*$^{-/-}$ than in the wt C57Bl/6 host, and number of lung metastases was about four times larger in KO than in wt mice. In the P2X7R-KO BALB/cJ strain growth rate was even faster compared to the wt, further highlighting the fundamental contribution of host P2X7R to the control of tumor growth. In fact, the C57Bl/6 strain is homozygous for a loss-of-function mutation causing a P415L substitution encoding a hypofunctional P2X7R (21). This puts C57Bl/6 mice somewhat halfway between a P2X7R-wt and a P2X7R-KO strain. On the contrary, the BALB/cJ strain carries the fully functional wt P2X7R, thus phenotypic differences with the KO are more clear cut.

A main cause for the inability of *p2x7R*$^{-/-}$ hosts to control tumor progression is likely to be the patent lack of an anti-tumor immune response. The crucial role of P2X7R expression on host hematopoietic cells in anti-tumor response was further confirmed by generating P2X7R chimeric mice. P2X7R-KO>P2X7R-wt chimeras allowed a much faster tumor growth than P2X7R-wt>P2X7R-KO chimeras, thus closely replicating tumor growth kinetics observed in the P2X7R-KO host. Accordingly, P2X7R-KO>P2X7R-KO mice allowed a faster tumor growth than P2X7R-wt>P2X7R-wt mice. While in the P2X7R-wt host the tumor was heavily infiltrated by $CD8^+$ lymphocytes and mononuclear phagocytes, in the P2X7R-KO host both the primary tumor and the metastatic sites showed virtually no inflammatory cell infiltrate. Thus, we were unable to characterize infiltrating immune cells in the specimens from the P2X7R-KO mice. Intra-mass levels of IL-1β and VEGF, two factors known to be released in response to P2X7R stimulation (44), (45)), were accordingly much lower in tumors growing in *p2x7R*$^{-/-}$ than in wt mice. Interestingly, while blood IL-1β was almost absent in the KO host, as expected on the basis of the known phenotype of the P2X7R-KO mouse, intra-mass IL-1β levels were elevated, although not to the same level as in the wt host. This discrepancy between intra-tumor and peripheral IL-1β levels is likely due to the intrinsic IL-1β-releasing activity of B16 melanoma (see also (23). Inability of the P2X7R-deleted host to release IL-1β was confirmed by direct *in vitro* stimulation of bone marrow-derived DCs

with B16 melanoma cells. Lack or response of immune cells from P2X7R-KO mice to stimulation with tumor cells is in keeping with previous results showing that mouse DCs lacking P2X7R fail to secrete IL-1β and to stimulate Ag-specific T_H lymphocytes (13).

In addition, P2X7R-deleted cells showed a reduced ability to migrate in a typical *in vitro* wound repair model, suggesting that lack of P2X7R hinders cell chemotaxis and thus tumor infiltration. The P2X7R itself, at variance with other P2 receptors, is not currently considered a chemotactic receptor but rather a membrane pathway that, by allowing ATP release, enhances the ATP-based chemotactic gradient (46), (37). An efficient ATP-based chemotaxis requires a controlled nucleotide release at the leading edge of the chemotacting cell (46), a process that might be highly inefficient in the absence of P2X7R.

Given the key role of host P2X7R in the anti-tumor immune responses highlighted in the present study, use of P2X7R blockers for anti-cancer therapy might appear problematic. We previously showed that that intramass injection of P2X7R inhibitors is an effective anti-tumor treatment (5), however, it might be objected that by injecting P2X7R blockers directly into the tumor, blockade of tumor P2X7R was maximized while possible inhibitory effects on host P2X7R were minimized. We now show that i.p. (systemic) administration of P2X7R antagonists was as effective as intra-mass injection. Since P2X7R blockade has an immunodepressive activity, it appears conceivable that a mild immunodepressive effect is the price to be paid to achieve anti-cancer activity.

Finally, our study shows that in an animal model genetically deleted of a receptor implicated in innate immunity, tumor growth and metastatic spreading are accelerated, thus highlighting the complex role of inflammation in host-tumor interaction.

In conclusion, we have identified P2X7R as a non redundant host factor in *in vivo* anticancer response.

References

1. Burnstock G. Physiology and pathophysiology of purinergic neurotransmission. Physiol Rev 2007;87:659-797.

2. Bours MJ, Dagnelie PC, Giuliani AL, Wesselius A, Di Virgilio F. P2 receptors and extracellular ATP: a novel homeostatic pathway in inflammation. Front Biosci (Schol Ed) 2011;3:1443-56.

3. Di Virgilio F. The P2Z purinoceptor: an intriguing role in immunity, inflammation and cell death. Immunol Today 1995;16:524-8.

4. Di Virgilio F. Purines, purinergic receptors, and cancer. Cancer Res 2012;72:5441-7.

5. Adinolfi E, Raffaghello L, Giuliani AL, Cavazzini L, Capece M, Chiozzi P, et al. Expression of the P2X7 receptor increases in vivo tumor growth. Cancer Res 2012;75:2957-2969.

6. Aymeric L, Apetoh L, Ghiringhelli F, Tesniere A, Martins I, Kroemer G, et al. Tumor cell death and ATP release prime dendritic cells and efficient anticancer immunity. Cancer Res 2010;70:855-8.

7. Bours MJ, Dagnelie PC, Giuliani AL, Wesselius A, Di Virgilio F. P2 receptors and extracellular ATP: a novel homeostatic pathway in inflammation. Front Biosci (Schol Ed) 2011;3:1443-56.

8. Wilhelm K, Ganesan J, Muller T, Durr C, Grimm M, Beilhack A, et al. Graft-versus-host disease is enhanced by extracellular ATP activating P2X7R. Nat Med 2010;16:1434-8.

9. Vergani A, Tezza S, D'Addio F, Fotino C, Liu K, Niewczas M, et al. Long-term heart transplant survival by targeting the ionotropic purinergic receptor P2X7. Circulation 2013;127:463-75.

10. Vergani A, Fotino C, D'Addio F, Tezza S, Podetta M, Gatti F, et al. Effect of the purinergic inhibitor oxidized ATP in a model of islet allograft rejection. Diabetes 2013;62:1665-75.

11. Adinolfi E, Raffaghello L, Giuliani AL, Cavazzini L, Capece M, Chiozzi P, et al. Expression of P2X7 receptor increases in vivo tumor growth. Cancer Res 2012;72:2957-69.

12. Michaud M, Martins I, Sukkurwala AQ, Adjemian S, Ma Y, Pellegatti P, et al. Autophagy-dependent anticancer immune responses induced by chemotherapeutic agents in mice. Science 2011;334:1573-7.

13. Mutini C, Falzoni S, Ferrari D, Chiozzi P, Morelli A, Baricordi OR, et al. Mouse dendritic cells express the P2X7 purinergic receptor: characterization and possible participation in antigen presentation. J Immunol 1999;163:1958-65.

14. Diaz-Hernandez M, del PA, Diaz-Hernandez JI, Diez-Zaera M, Lucas JJ, Garrido JJ, et al. Inhibition of the ATP-gated P2X7 receptor promotes axonal growth and branching in cultured hippocampal neurons. J Cell Sci 2008;121:3717-28.

15. Syberg S, Petersen S, Beck Jensen JE, Gartland A, Teilmann J, Chessell I, et al. Genetic Background Strongly Influences the Bone Phenotype of P2X7 Receptor Knockout Mice. J Osteoporos 2012;2012:391097.

16. Sjoo F, Hassan Z, Abedi-Valugerdi M, Griskevicius L, Nilsson C, Remberger M, et al. Myeloablative and immunosuppressive properties of treosulfan in mice. Exp Hematol 2006;34:115-21.

17. Sangaletti S, Stoppacciaro A, Guiducci C, Torrisi MR, Colombo MP. Leukocyte, rather than tumor-produced SPARC, determines stroma and collagen type IV deposition in mammary carcinoma. J Exp Med 2003;198:1475-85.

18. Inaba K, Inaba M, Romani N, Aya H, Deguchi M, Ikehara S, et al. Generation of large numbers of dendritic cells from mouse bone marrow cultures supplemented with granulocyte/macrophage colony-stimulating factor. J Exp Med 1992;176:1693-702.

19. Giuliani AL, Wiener E, Lee MJ, Brown IN, Berti G, Wickramasinghe SN. Changes in murine bone marrow macrophages and erythroid burst-forming cells following the intravenous injection of liposome-encapsulated dichloromethylene diphosphonate (Cl2MDP). Eur J Haematol 2001;66:221-9.

20. Lemaire I, Falzoni S, Zhang B, Pellegatti P, Di Virgilio F. The P2X7 receptor and Pannexin-1 are both required for the promotion of multinucleated macrophages by the inflammatory cytokine GM-CSF. J Immunol 2011;187:3878-87.

21. Adriouch S, Dox C, Welge V, Seman M, Koch-Nolte F, Haag F. Cutting edge: a natural P451L mutation in the cytoplasmic domain impairs the function of the mouse P2X7 receptor. J Immunol 2002;169:4108-12.

22. Dinarello CA. A clinical perspective of IL-1beta as the gatekeeper of inflammation. Eur J Immunol 2011;41:1203-17.

23. Dunn JH, Ellis LZ, Fujita M. Inflammasomes as molecular mediators of inflammation and cancer: potential role in melanoma. Cancer Lett 2012;314:24-33.

24. Ferrari D, Villalba M, Chiozzi P, Falzoni S, Ricciardi-Castagnoli P, Di Virgilio F. Mouse microglial cells express a plasma membrane pore gated by extracellular ATP. J Immunol 1996;156:1531-9.

25. Labasi JM, Petrushova N, Donovan C, McCurdy S, Lira P, Payette MM, et al. Absence of the P2X7 Receptor Alters Leukocyte Function and Attenuates an Inflammatory Response. J Immunol 2002;168:6436-45.

26. Barbera-Cremades M, Baroja-Mazo A, Gomez AI, Machado F, Di Virgilio F, Pelegrin P. P2X7 receptor-stimulation causes fever via PGE2 and IL-1beta release. FASEB J 2012;26:2951-62.

27. Asgari E, Le FG, Yamamoto H, Perucha E, Sacks SS, Kohl J, et al. C3a modulates IL-1beta secretion in human monocytes by regulating ATP efflux and subsequent NLRP3 inflammasome activation. Blood 2013;122:3473-81.

28. Quail DF, Joyce JA. Microenvironmental regulation of tumor progression and metastasis. Nat Med 2013;19:1423-37.

29. Pellegatti P, Raffaghello L, Bianchi G, Piccardi F, Pistoia V, Di Virgilio F. Increased level of extracellular ATP at tumor sites: in vivo imaging with plasma membrane luciferase. PLoS ONE 2008;3:e2599.

30. Forrester T. An estimate of adenosine triphosphate release into the venous effluent from exercising human forearm muscle. J Physiol 1972;224:611-28.

31. Falzoni S, Donvito G, Di Virgilio F. Detecting adenosine triphosphate in the pericellular space. Interface Focus 2013;3:20120101.

32. Ralevic V, Burnstock G. Receptors for purines and pyrimidines. Pharmacol Rev 1998;50:413-92.

33. North RA. Molecular physiology of P2X receptors. Physiol Rev 2002;82:1013-67.

34. Gu BJ, Wiley JS. Rapid ATP-induced release of matrix metalloproteinase 9 is mediated by the P2X7 receptor. Blood 2006;107:4946-53.

35. Coutinho-Silva R, Correa G, Sater AA, Ojcius DM. The P2X(7) receptor and intracellular pathogens: a continuing struggle. Purinergic Signal 2009;5:197-204.

36. Di Virgilio F. Dr. Jekyll/Mr. Hyde: the dual role of extracellular ATP. J Auton Nerv Syst 2000;81:59-63.

37. Rayah A, Kanellopoulos JM, Di Virgilio F. P2 receptors and immunity. Microbes Infect 2012;14:1254-62.

38. Adinolfi E, Callegari MG, Ferrari D, Bolognesi C, Minelli M, Wieckowski MR, et al. Basal Activation of the P2X7 ATP Receptor Elevates Mitochondrial Calcium and Potential, Increases Cellular ATP Levels, and Promotes Serum-independent Growth. Mol Biol Cell 2005;16:3260-72.

39. Bianco F, Ceruti S, Colombo A, Fumagalli M, Ferrari D, Pizzirani C, et al. A role for P2X7 in microglial proliferation. J Neurochem 2006;99:745-58.

40. Monif M, Reid CA, Powell KL, Smart ML, Williams DA. The P2X7 Receptor Drives Microglial Activation and Proliferation: A Trophic Role for P2X7R Pore. J Neurosci 2009;29:3781-91.

41. Burnstock G, Di Virgilio F. Purinergic signalling and cancer. Purinergic Signal 2013;9:491-540.

42. Adinolfi E, Cirillo M, Woltersdorf R, Falzoni S, Chiozzi P, Pellegatti P, et al. Trophic activity of a naturally occurring truncated isoform of the P2X7 receptor. FASEB J 2010;24:3393-404.

43. Ghalali A, Wiklund F, Zheng H, Stenius U, Hogberg J. Atorvastatin prevents ATP-driven invasiveness via P2X7 and EHBP1 signaling in PTEN-expressing prostate cancer cells. Carcinogenesis 2014.

44. Ferrari D, Chiozzi P, Falzoni S, Dal Susino M, Melchiorri L, Baricordi OR, et al. Extracellular ATP triggers IL-1 beta release by activating the purinergic P2Z receptor of human macrophages. J Immunol 1997;159:1451-8.

45. Hill LM, Gavala ML, Lenertz LY, Bertics PJ. Extracellular ATP may contribute to tissue repair by rapidly stimulating purinergic receptor X7-dependent vascular endothelial growth factor release from primary human monocytes. J Immunol 2010;185:3028-34.

46. Junger WG. Immune cell regulation by autocrine purinergic signalling. Nat Rev Immunol 2011;11:201-12.

Figure legends

Figure 1 Accelerated tumor growth in P2X7R-KO mice. A, P2X7R-KO or wt C57Bl/6 mice (n = 6) were inoculated into the right hind leg with B16 cells (5×10^5) stably transfected with cytosolic luciferase (cytLuc). In some experiments, tumor cells were co-transfected with both cytLuc and P2X7R-shRNA (P2X7R-silenced cells). Tumor volume was *in vivo* assessed by calliper at the indicated p.i. time points. B, representative pictures of P2X7R-expressing (upper panel) or P2X7R-silenced (lower panel) tumors from wt or P2X7R-KO mice at p.i. day 14. C and D, kinetics of tumor growth in wt and P2X7R-KO mice estimated by cytLuc luminescence emission (photon/second, p/s) at the indicated p.i. days. E, BALB/cj mice (n = 6) were subcutaneously inoculated into the right hind leg with CT26 cells (2.5×10^5). Tumor volume was *in vivo* assessed by calliper. F, *post-mortem* tumor size. G, representative picture of tumor masses from and P2X7R-KO and wt mice. Data are averages $\pm$ SEM. A, * $p < 0.05$, ** $p < 0.01$, *** $p < 0.001$ vs P2X7R-wt+B16-wt; § $p < 0.05$, §§ $p < 0.01$ vs P2X7R-wt+B16-shRNA. # $p < 0.05$ vs P2X7R-wt shRNA. D, E and F, * $p < 0.05$.

Figure 2 Lung metastases of B16 melanoma in wt and P2X7R-KO mice assessed by luminescence emission. Six wt (A) or P2X7R-KO (B) mice at p.i. day 18 are shown. Numbers (#) below panels indicate mouse number. C, kinetics of lung metastases dissemination assessed by luminescence at the indicated p.i. days. D, lungs from wt and P2X7R-KO mice shown in panel C and sacrificed at p.i. d 21. Panel E. Average $\pm$ SEM lung metastases number in wt and P2X7R-KO mice. E, * $p < 0.05$.

Figure 3 Lack of inflammatory infiltrate in tumors from primary B16 melanomas grown in P2X7R-KO mouse. Specimens from P2X7R-KO (A-C) or wt (D-F) mice were stained with H/E as described in Materials and Methods.

Figure 4 B16 melanomas growing in the P2X7R-KO host lack T lymphocyte and macrophage infiltrate. A and B, primary B16 tumor from P2X7R-KO or wt mice, respectively, stained with anti-CD3 Ab. C and D, primary B16 tumor from P2X7R-KO or wt mice, respectively, stained with anti-F4/80 mAb. E and F, B16 primary tumor from P2X7R-wt host stained with aanti-$CD8^+$ mAb. Samples were stained with H/E as described in Materials and Methods.

Figure 5 Lung metastases of B16 melanoma from P2X7R-KO mice lack inflammatory cell infiltration. Specimens from P2X7R-KO (A-C) or wt mice (D-F). Specimens A, B, D, and E were fixed and stained with H/E, while specimens C and F were stained with anti-CD3 Ab without previous H/E staining.

Figure 6 Analysis of tumor growth in P2X7R-KO>P2X7R-wt chimeras, Interleukin-1β release and effect of P2X7R blockade. A, Tumor growth in P2X7R-wt>P2X7R-KO, P2X7R-KO>P2X7R-wt, P2X7R-KO>P2X7R-KO, and P2X7R-wt>P2X7R-wt chimeric mice. BMT was performed as described in Materials and Methods. Data are averages ± SEM (n = 4). * $p < 0.05$, ** $p < 0.01$ for P2X7R-KO>P2X7R-wt versus P2X7R-wt>P2X7R-wt, by one tail unpaired t-test. B, IL-1β plasma levels. C, intra-tumor IL-1β levels. D, IL-1β release from B16-challenged DCs isolated from wt or P2X7R-KO mice. Data are averages $\pm$ SEM (n = 5). B, C, * $p < 0.05$, ** $p < 0.01$, for P2X7R-KO vs P2X7R-wt; C, # $p < 0.05$ for P2X7R-KO+B16shRNA vs P2X7R-wt+B16 shRNA. E-G, effect of i.p. administration of P2X7R blockers on tumor growth in the P2X7R-wt host. Mice were inoculated with B16 cells (5×10^5) as described in Figure 1 and, starting at day 5, i.p. injected every two days with 100 µl of A74003 (10 µM), AZ10606120 (300 nM) or placebo. E, *in vivo* kinetics of tumor growth. F, tumor size after *post-mortem* excision. G, representative picture of tumor masses from placebo and P2X7R antagonist-injected mice. Data are averages ± SEM (n = 5). * $p < 0.05$ vs placebo.

Figure 7 P2X7-less N13 mouse microglia cells have impaired wound-healing ability. N13 and N13R cells were seeded in Petri dishes and allowed to reach confluence before scratching. At this point, the monolayer was scratched with a pipette tip and cell migration recorded for 16 h.

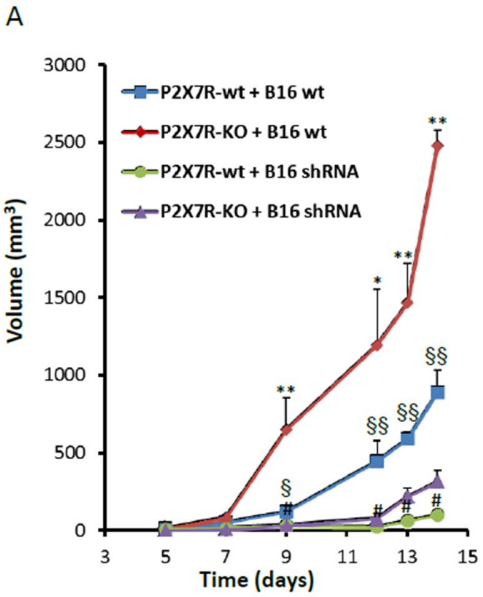

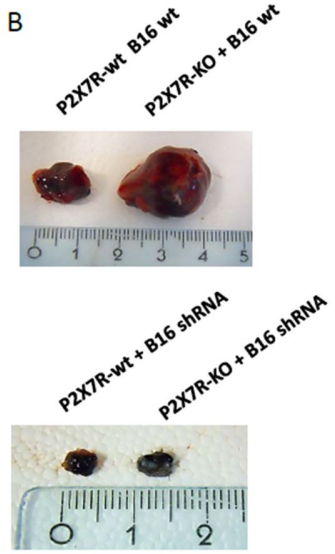

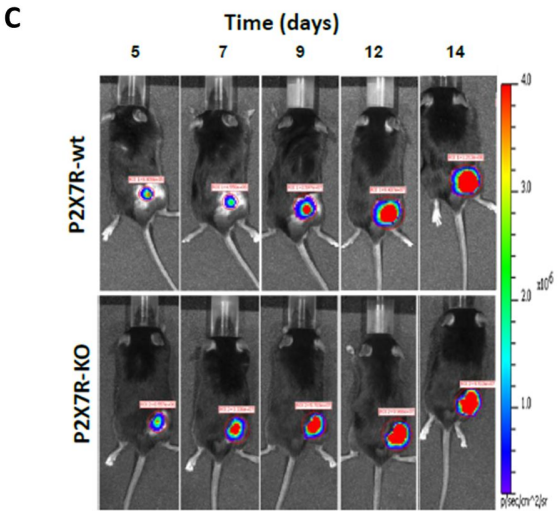

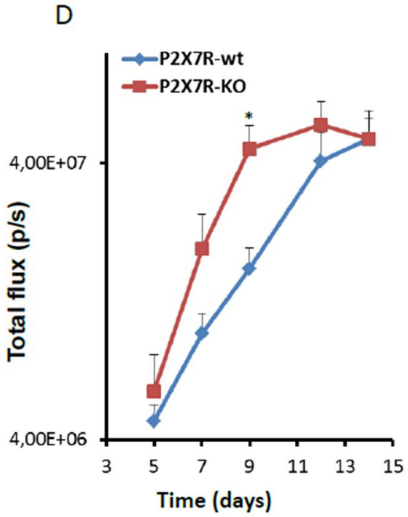

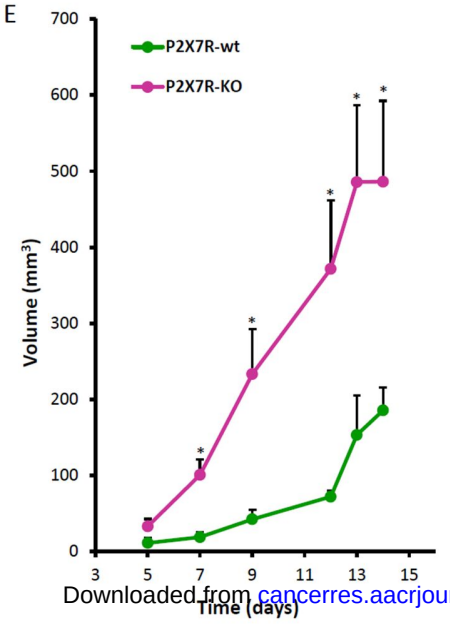

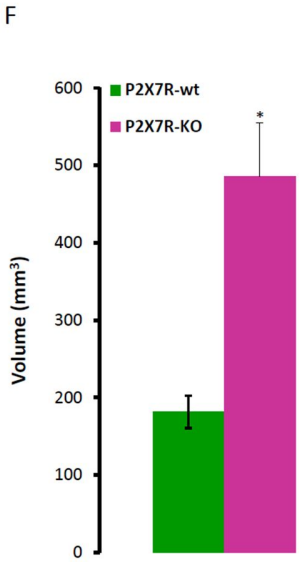

Figure 1

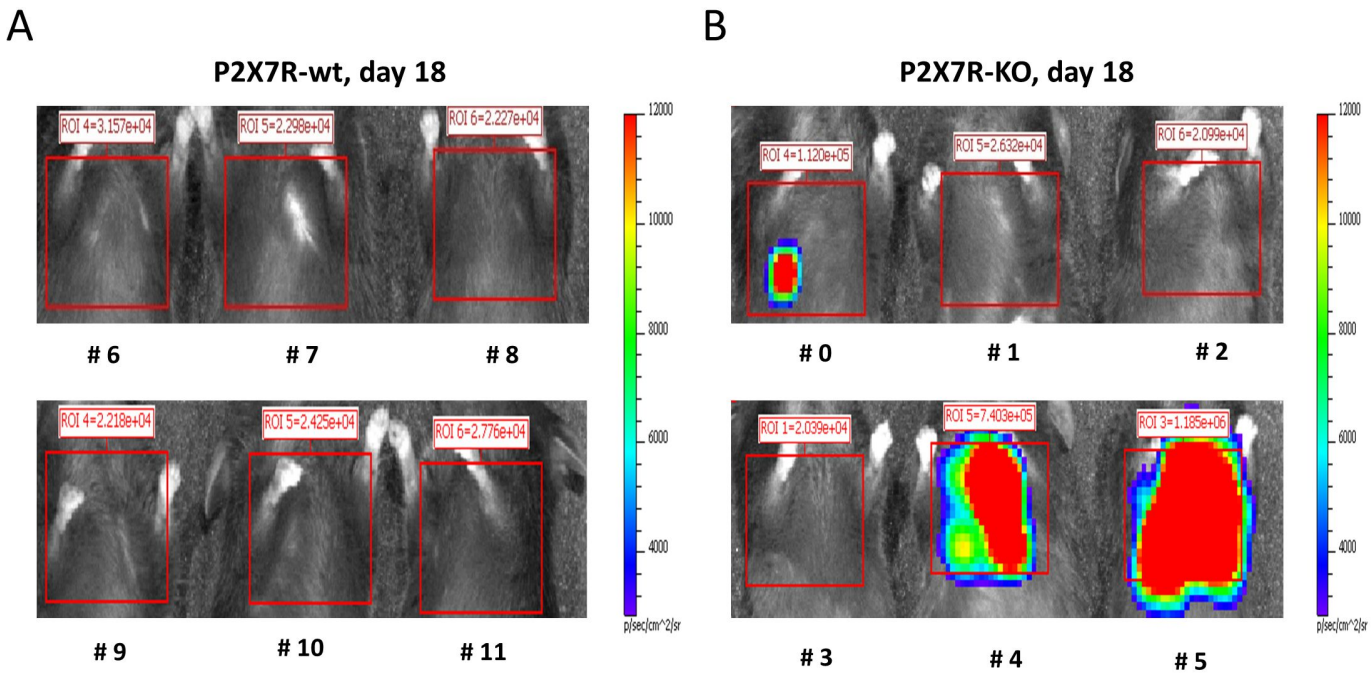

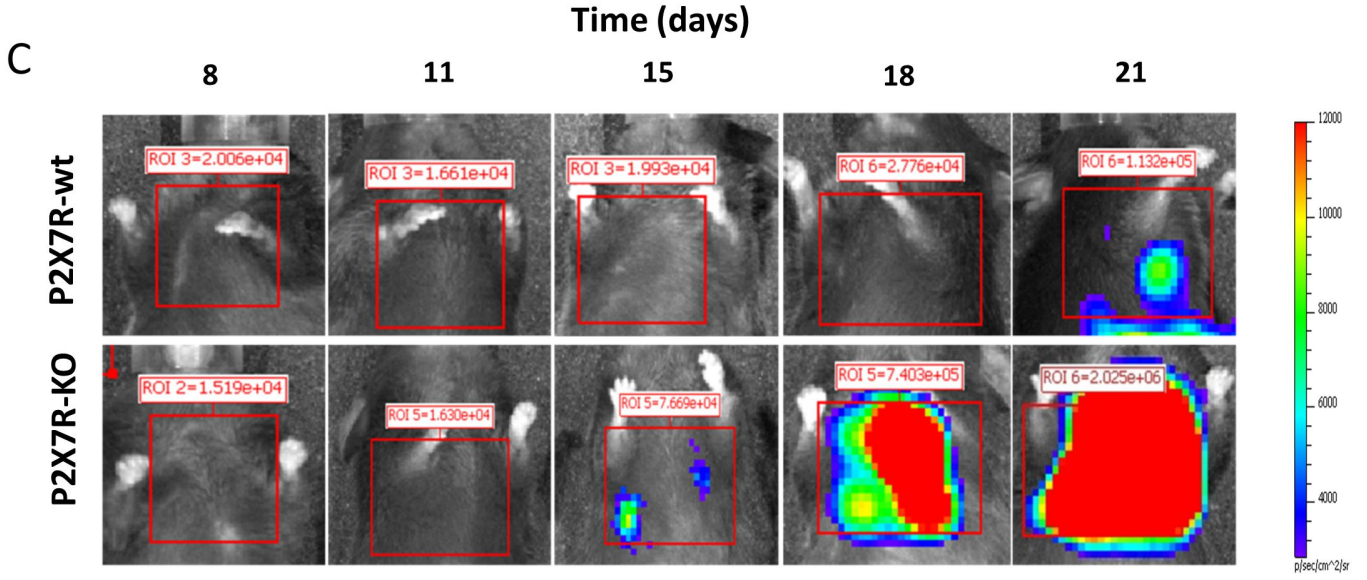

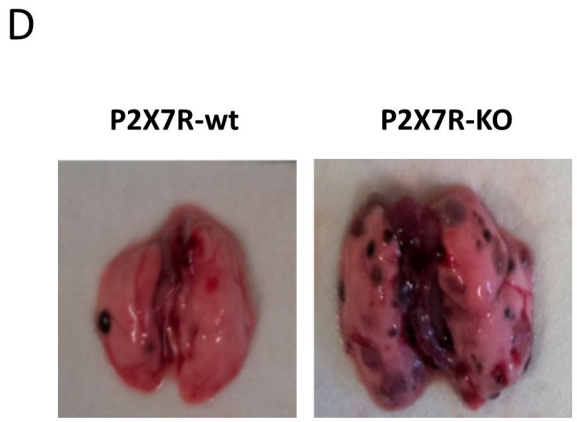

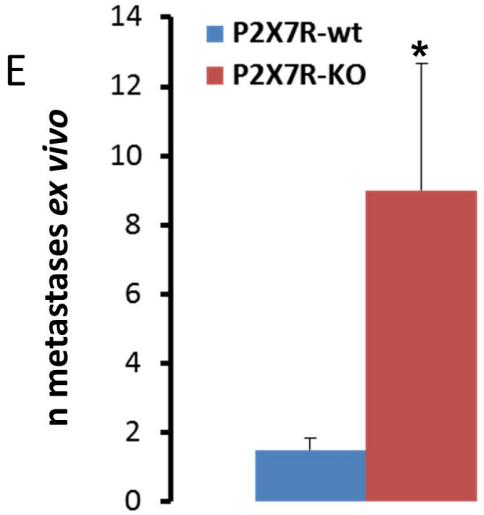

Figure 2

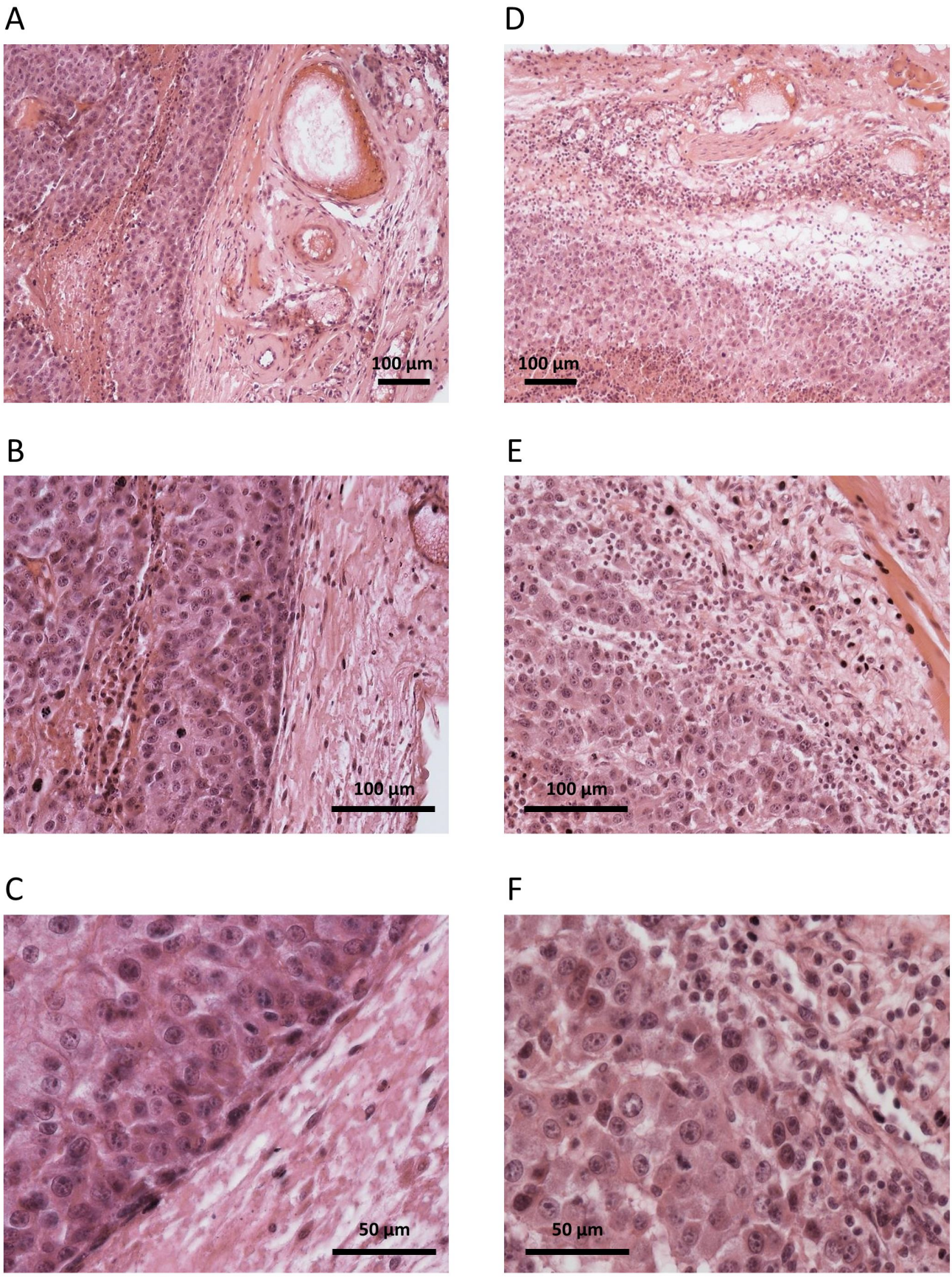

Figure 3

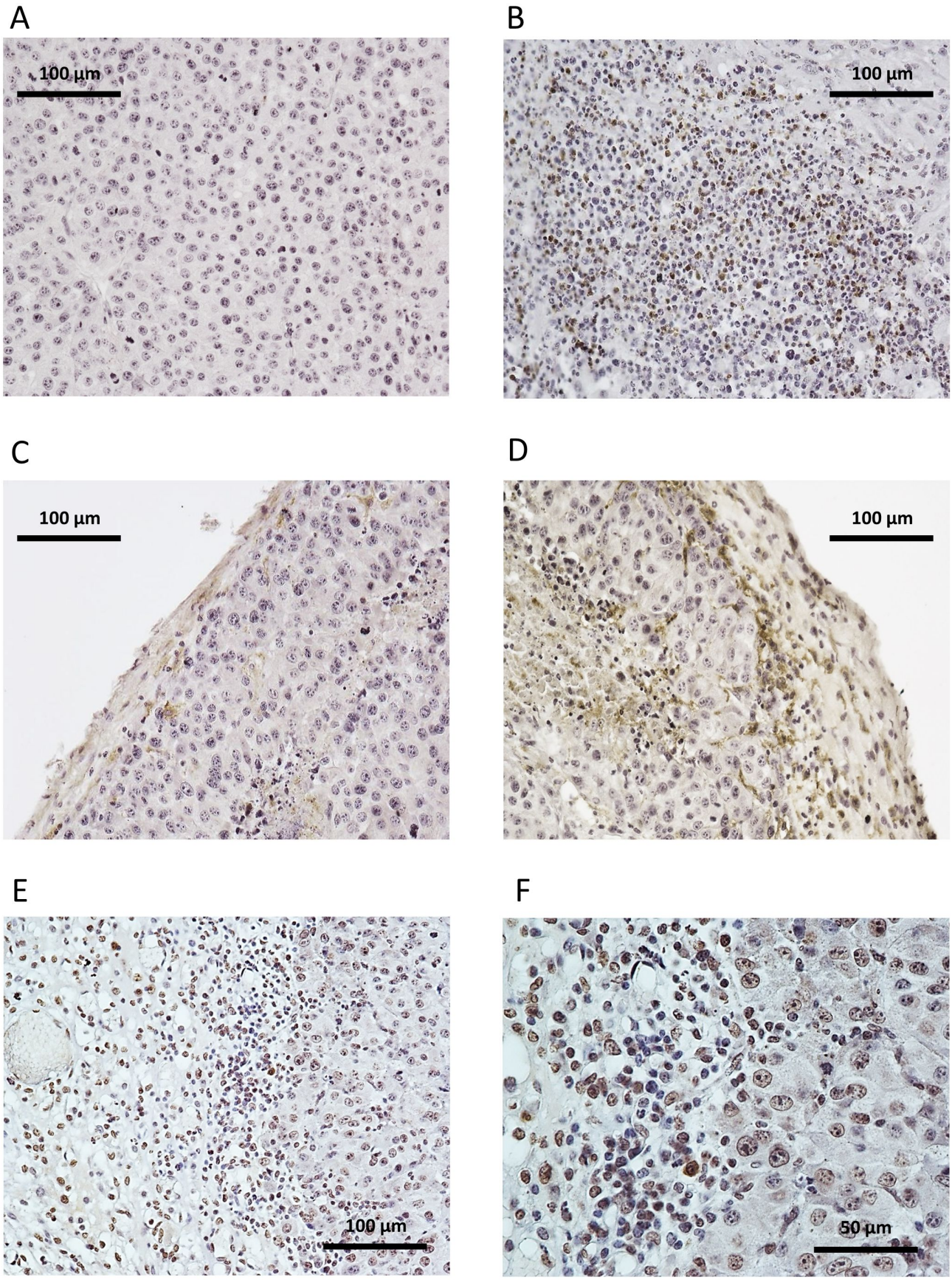

Fig. 4

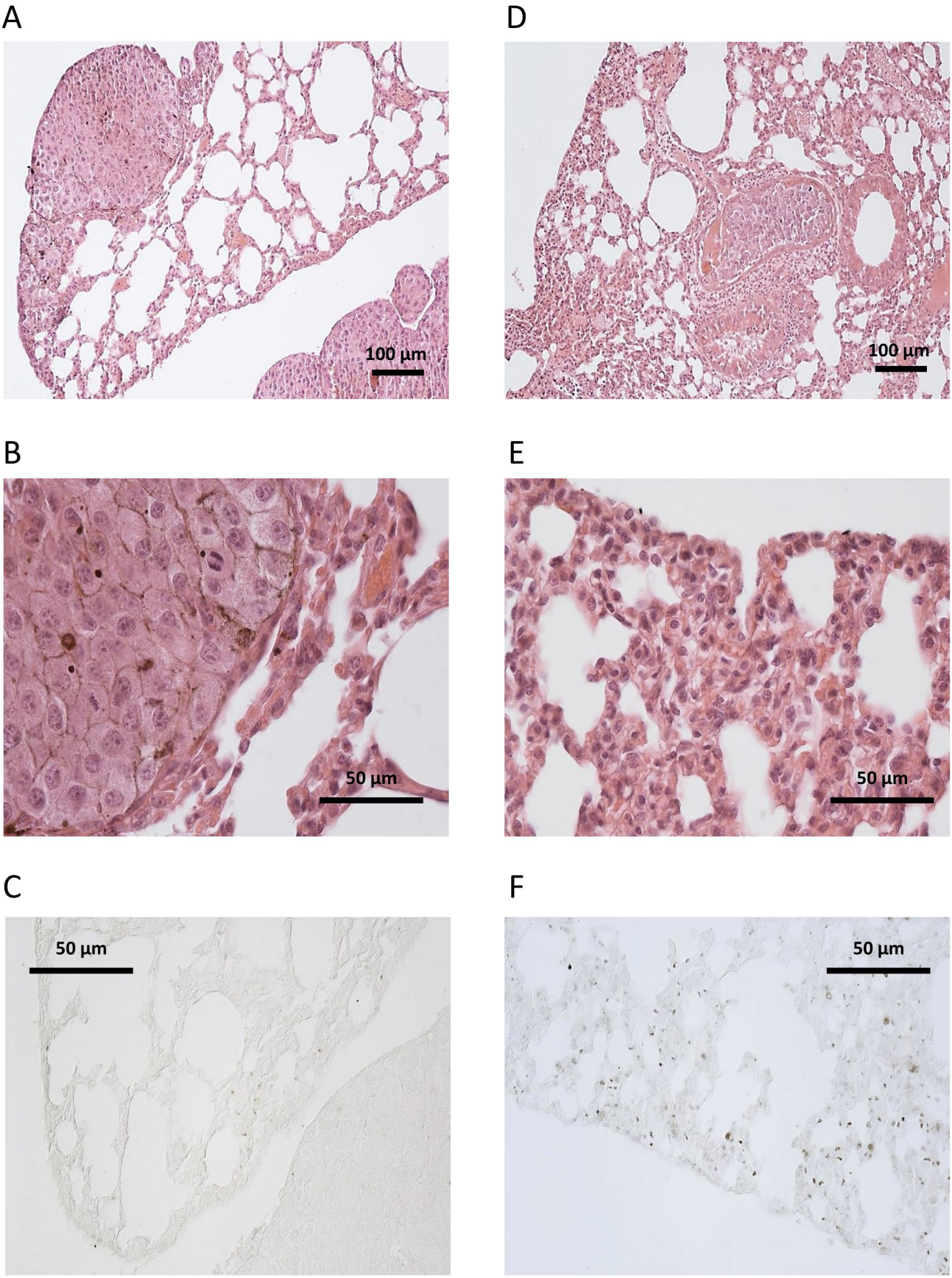

Fig. 5

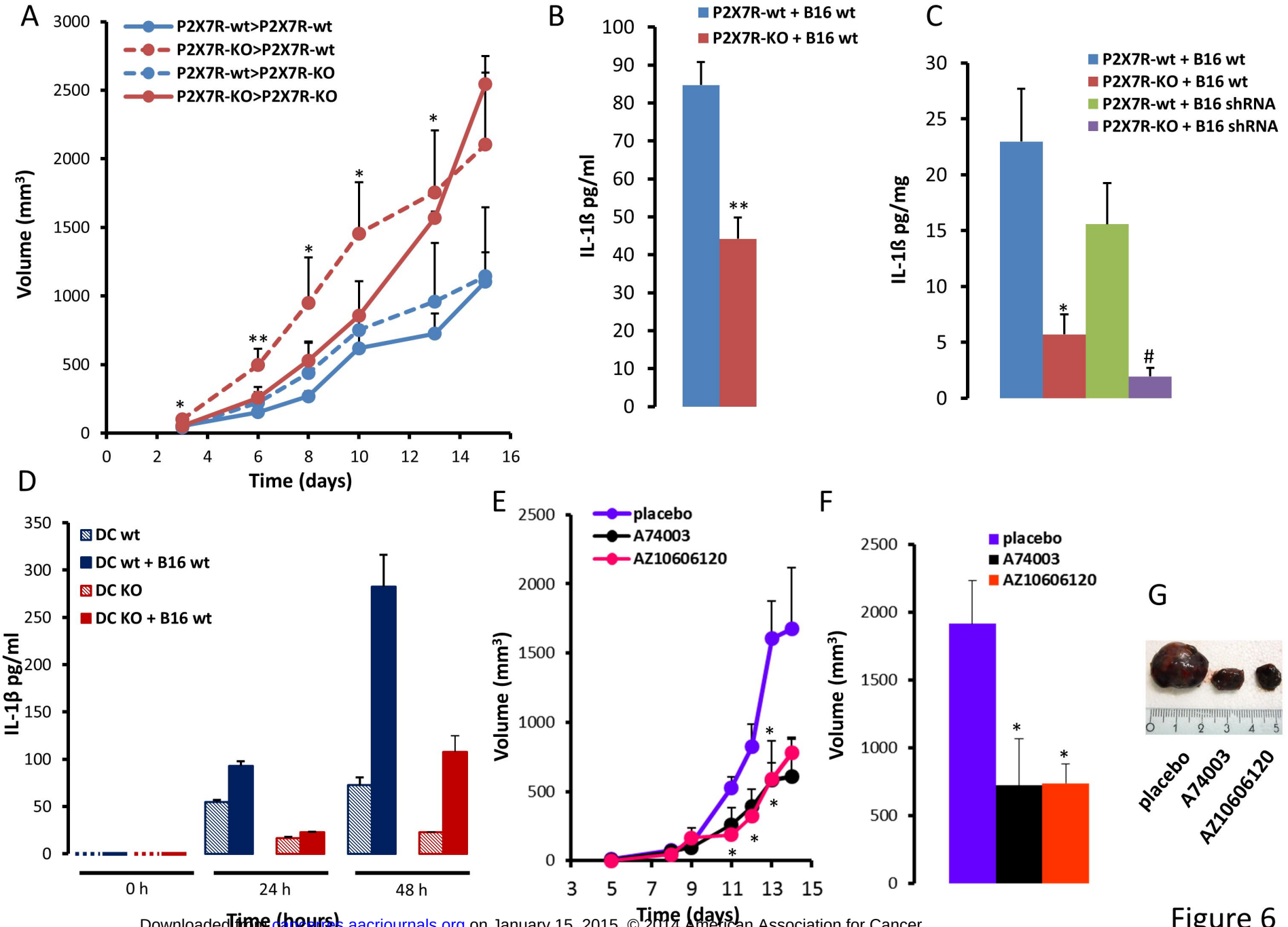

Figure 6

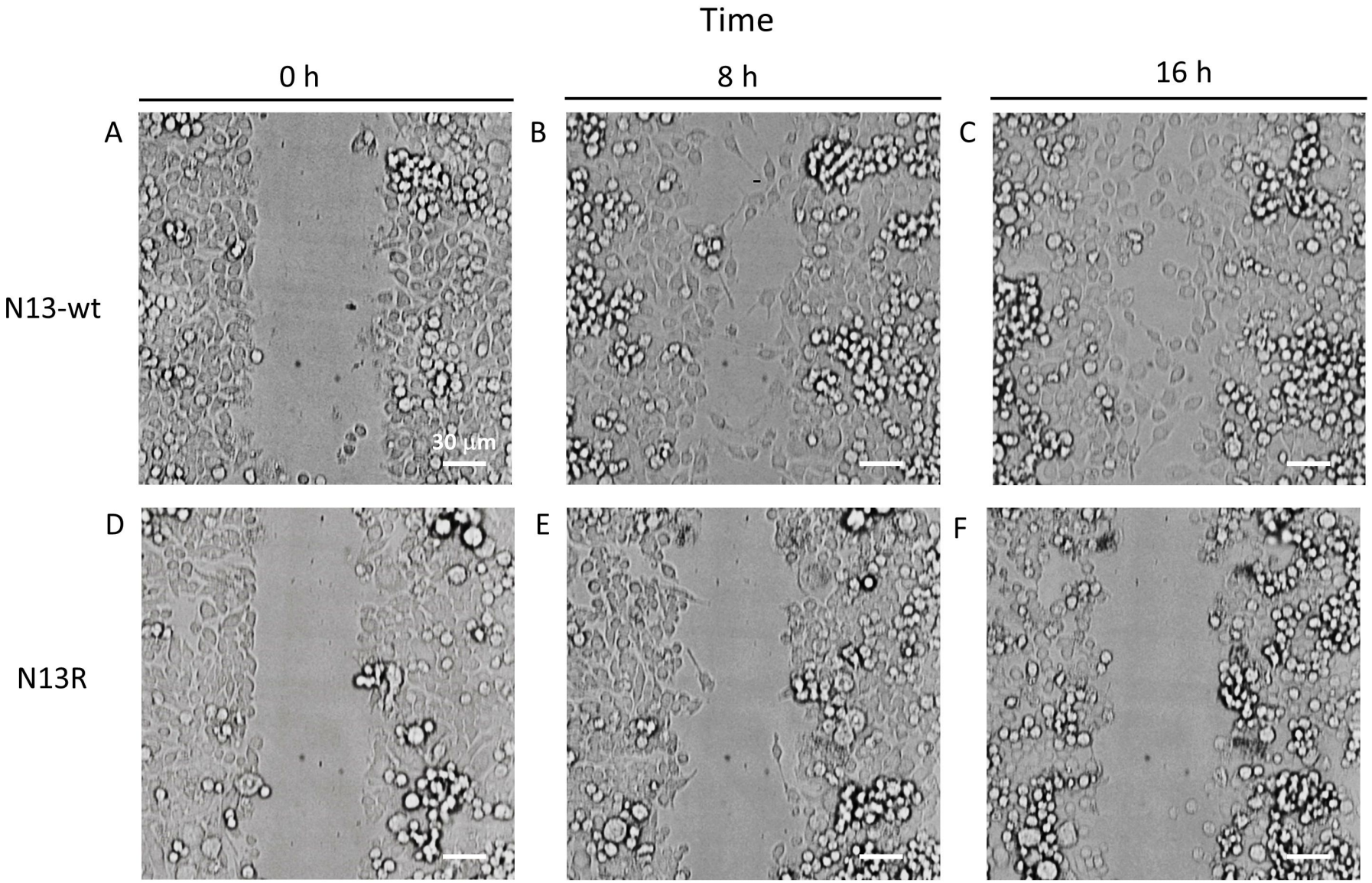

Figure 7

Cancer Research

Accelerated tumor progression in mice lacking the P2X7 receptor

Elena Adinolfi, Marina Capece, Alessia Franceschini, et al.

Cancer Res Published OnlineFirst December 26, 2014.